Journal of *Marine Science and Engineering*

MDPI

Article

Numerical Simulation of Natural Gas Hydrate Depressurization Extraction Considering Phase Transition Characteristics

Qiang Fu [1,2], Mingqiang Chen [1,2,*], Weixin Pang [1,2] and Lirong Dong [3]

[1] State Key Laboratory of Offshore Natural Gas Hydrate, China National Offshore Oil Corporation, Beijing 100028, China; fuqiang8@cnooc.com.cn (Q.F.); pangwx@cnooc.com.cn (W.P.)
[2] Research Institute of China National Offshore Oil Corporation, China National Offshore Oil Corporation, Beijing 100028, China
[3] Department of Petroleum Engineering, China University of Petroleum (Beijing), Beijing 102249, China; 2024310213@student.cup.edu.cn
* Correspondence: chenmq17@cnooc.com.cn

Abstract: Natural gas hydrate (NGH) is a clean resource characterized by abundant potential reserves, clean combustion, and high energy density. Although significant progress has been made in the development of NGH resources all around the world, challenges still exist that hinder commercial exploitation, such as a low daily gas production rate and short steady production periods. One significant reason lies in the complex gas–liquid–solid phase transitions occurring within the formation during production, which lead to changes in flow capacity. Understanding the phase change mechanism of NGH reservoirs will help to further reveal the production increase mechanism. To address the phase transitions' effect on production, this paper establishes a numerical simulation model for the depressurization exploitation of natural gas hydrates in order to investigate phase transition characteristics at the field scale. First, the phase equilibrium calculation method is presented and the phase equilibrium curve is modified by considering the capillary effect, soluble salt, and surface adsorption. Then, the phase transition model is successfully characterized in a simulation and the numerical simulation model is established based on the first test project parameters in the Shenhu area. The production characteristics of different sediment types (montmorillonite, South China Sea sediments, kaolin, and silt) are analyzed under the effects of water content and salinity. It is shown that lower initial water content and higher salinity result in higher gas production. The results provide a better understanding of the effects of phase transition parameters on NGH production at the field scale.

Keywords: natural gas hydrate; phase transition characteristics; numerical simulation; depressurization exploitation

check for updates

Academic Editor: Dejan Brkić

Received: 8 February 2025
Revised: 24 February 2025
Accepted: 24 February 2025
Published: 5 March 2025

Citation: Fu, Q.; Chen, M.; Pang, W.; Dong, L. Numerical Simulation of Natural Gas Hydrate Depressurization Extraction Considering Phase Transition Characteristics. *J. Mar. Sci. Eng.* **2025**, *13*, 511. https://doi.org/10.3390/jmse13030511

Copyright: © 2025 by the authors. Licensee MDPI, Basel, Switzerland. This article is an open access article distributed under the terms and conditions of the Creative Commons Attribution (CC BY) license (https://creativecommons.org/licenses/by/4.0/).

1. Introduction

Natural gas hydrate, which is known as "combustible ice", is a compound resembling ice that forms from CH_4 molecules (primarily methane) and water molecules under high-pressure and low-temperature conditions. It has a high energy density, with 1 m^3 of natural gas hydrate being capable of releasing approximately 164 m^3 of natural gas and 0.8 m^3 of water upon decomposition. Compared to traditional fossil fuels such as coal and oil, its combustion produces significantly fewer pollutants. Natural gas hydrates are primarily found in soft sediment layers located at depths ranging from 300 m underwater to approximately 1500 m beneath the seabed. Additionally, fewer amounts have been discovered in terrestrial permafrost regions. It is estimated that the reserves of natural gas

hydrates amount to about 2.1×10^{16} m^3 in the world, roughly twice the total reserves of other fossil energy sources [1].

As a new clean energy source with abundant reserves, clean combustion, and high energy density, natural gas hydrates have attracted widespread attention and in-depth research globally for many years [2–4]. Japan has conducted two production activity tests focused on hydrates. It has been proven that the depressurization method is the most suitable for hydrate development. In the test project, Japan proposed a series of measures to prevent geological hazards and thereby increase the production rate [5]. The U.S. Department of Energy carried out a trial of NGH production in the permafrost region of Alaska's North Slope, with test results showing that the method of replacing CH_4 with CO_2 is a practical and effective exploitation strategy [6]. Although China started to conduct test research on natural gas hydrate production relatively late, it is the only country to have successfully conducted production trials in both marine and terrestrial regions. In 1990, the Lanzhou Institute of Glaciology and Geocryology of the Chinese Academy of Sciences achieved the pioneering artificial synthesis of hydrates and began studying natural gas hydrates in the permafrost layer of the Qinghai–Tibet Plateau [7], estimating the resource amount at 1.2×10^{11} m^3 to 2.4×10^{14} m^3 [8]. Geological surveys indicate that China's marine areas are extremely rich in NGH resources, especially in the northern slope region of the South China Sea, where prospective hydrate resources are estimated to be as high as 18.458 billion tons of oil equivalent [9]. On 29 July 2017, an offshore production test project concerning NGHs in the Shenhu area of the South China Sea, conducted by the China Geological Survey under the Ministry of Land and Resources, was successfully completed. During this test, the cumulative gas production reached 309,000 m^3, with an average daily production of 5151 m^3 and a peak daily production of 35,000 m^3. This achievement marked the successful completion of China's first offshore trial of NGH production [10]. In February 2020, China's second trial round of offshore NGH production was also a resounding success, setting new world records for "cumulative gas production" and "average daily gas production", recording a solid step forward from preliminary exploration to the real production test stage [11].

Although significant progress has been made by various countries in the exploitation of natural gas hydrate resources, challenges such as low daily gas production, short production stability periods, and the inability to meet the requirements for commercial exploitation have limited its economic feasibility and investment prospects [12]. The primary issue is that the phase transition of hydrates occurs throughout the whole production process, leading to complex gas–liquid–solid phase changes within the reservoir [13,14]. Additionally, changes in temperature, pressure, and fluid composition can result in the formation and deposition of hydrates within the reservoir. This hydrate formation can clog pores, reduce reservoir permeability, hinder the production of gas and water, and pose significant challenges to extraction. The risk of hydrate formation is particularly high in the low-temperature, high-pressure environment of the seabed. Clayey silt porous media, characterized by complex mineral compositions and heterogeneous pore structures, exert a compounded influence on the phase transition processes of hydrates. Furthermore, hydrate phase transitions can alter the formation of physical properties, such as porosity and permeability, which in turn impact gas production efficiency [15].

Due to the high cost of production tests and limited data availability, further experimental research and numerical simulations are essential. In 2015, Zang et al. elaborated on the core reasons for the influence of pore size on the pressure–temperature equilibrium conditions of hydrates, attributing it mainly to changes in the characteristics of adsorbed water and its surface tension induced by pore size. However, the specific mechanisms remain unclear [16]. Liu (2019), using molecular dynamics simulation, investigated the microscopic

mechanisms of natural gas hydrate decomposition in microporous environments. The flow characteristics of two-phase fluids within pores was analyzed, providing a detailed explanation of the microscopic mechanisms of hydrate production [17]. Later, a pore-throat scale study was performed to explore the decomposition mechanisms of hydrates. Utilizing micro-pore technologies with a two-dimensional porous silicon ship and simulating real sandstone pore structures, they successfully visualized hydrate decomposition during depressurization production [18]. Wan et al. applied Raman spectroscopy to study the decomposition processes of methane hydrates within nanoporous silica under atmospheric pressure and at multiple low temperatures (263 K, 253 K, 243 K), delving into the micro-decomposition characteristics of methane hydrates in confined nano-environments [19]. Kuang (2021) employed in situ liquid transmission electron microscopy and atomic force microscopy at microscale and nanoscale levels to capture and trace the Brownian motion trajectories of nanobubbles within water layers during hydrate phase decomposition for the first time. He proposed and validated the regulatory role of nanobubbles in the mass transfer process during hydrate phase decomposition [20]. Guan et al. reviewed changes in the phase equilibrium of hydrates in porous media with varying pore sizes and analyzed the specific effects of pore size on hydrate phase equilibrium. Their study revealed that the strong capillary forces generated in porous media reduce water activity, thereby inhibiting hydrate formation, with a critical threshold observed at the nanoscale [21].

Numerical simulation is a crucial tool for guiding hydrate development. It offers robust capabilities, flexible methodologies, and low costs, providing real-time insights into the evolution of physical and chemical parameters in reservoirs that are often unobservable in field experiments. For example, Wang et al. utilized the thermodynamic software CSMHYD to reveal that factors such as water depth, seabed temperature, gas composition, and pore water salinity significantly affect the phase equilibrium curve of NGHs [22]. Su et al. focused on the influence of various hydrocarbon components in natural gas on hydrate formation temperatures using the HYSYS software [23]. Li et al. calculated the effects of gas composition, pore water components, pore radius, microwave exposure, and surfactants on hydrate phase equilibrium using the CSMHYD program [24]. Ruan et al. developed a laboratory-scale mathematical model for depressurization exploitation of natural gas hydrates. This model simulated the secondary formation of hydrates during the depressurization process and analyzed the impact of this phenomenon, along with permeability changes, on gas production efficiency [25]. Han (2020), starting with the development of a numerical model for pore-scale hydrate behavior evolution, used nuclear magnetic resonance imaging to characterize pore structures in multiple sandstone cores. Subsequently, various forms of the Kozeny–Carman model were established to describe the relationship between porosity and permeability, enabling predictions of permeability under different natural gas hydrate occurrences [26]. Zhou et al. employed the Multiflash software to simulate the effects of factors such as gas composition, salts, inhibitors, temperature, and pressure on hydrate phase equilibrium. Their work provides theoretical support for flow assurance in hydrate exploration and development [27]. The permeability characteristics of natural gas hydrates in cores are influenced by their porous skeletal structure and change dynamically during hydrate phase transitions. The overall geological storage environment for hydrates, comprising hydrate-bearing sediment layers, overlying caps, and underlying basement formations, plays a critical role during hydrate decomposition. Xu et al. built geological system models with varying permeability characteristics. Numerical simulations revealed that enhancing cap-sealing properties and optimizing the permeability of hydrate-bearing sediments can lead to comprehensive improvements [28]. Chen (2021) constructed a 2D pore-scale ball-and-rod model using the numerical simulation tool Fluent, coupled with custom user-defined functions (UDFs). This model was applied to investi-

gate methane hydrate decomposition during depressurization under various conditions, including different decomposition pressures, initial hydrate temperatures, and pore-throat configurations [29].

Until now, the phase transition mechanisms that are present under complex environmental parameters were not completely clear [30,31]. This study analyzes the phase equilibrium curve, considering the capillary effect, surface adsorption, and soluble salt. The phase transition model then is coupled with the simulator. The simulation model is established using the depressurization production test data of natural gas hydrates in the Shenhu area of the South China Sea in 2017. The simulation integrates the phase change characteristics of NGHs and the gas production characteristics are analyzed. This is the first time a simulation has been used to describe phase transition in the sediment conditions of the South China Sea. The results provide a tool for hydrate phase behavior prediction and a workflow for numerical simulation regarding phase transition characteristics in clayey–silty sediments.

2. Analysis Model

2.1. Conditions of Study Region

The Shenhu area is located in the southeastern sea region, situated on the central section of the northern slope of the South China Sea. Geologically, it is part of the passive continental margin of the South China Sea, lying between the Xisha Trough and Dongsha Atoll. The specific location is shown in Figure 1. The seabed topography in the study area is highly undulating, with a complex and variable slope morphology that generally steps downward. The region features diverse geomorphological structures conducive to hydrate formation, including troughs, valleys, seamounts, knolls, steep slopes, escarpments, submarine plateaus, submarine landslides, and submarine fans. During the Cenozoic period, the northern continental margin of the South China Sea experienced several regional tectonic movements, such as the Shenhu, Zhuqiong, South China Sea, and Dongsha movements. As a result, the regional fault–fold system is well developed, with numerous faults penetrating newer sedimentary layers and extending near the seabed. These faults provide favorable pathways for natural gas migration to the shallow hydrate stability zone.

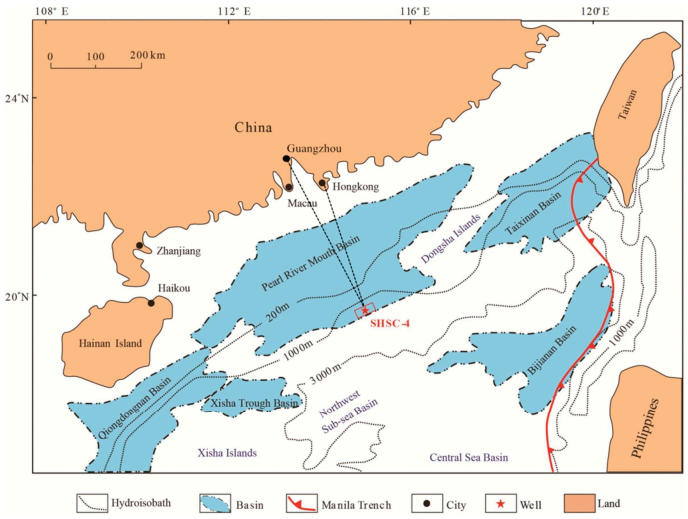


Figure 1. The first NGH production test location in the Shenhu area [32].

2.2. Model Description

Figure 2 depicts a schematic model of the first NGH production test conducted in the Shenhu area of the South China Sea. This study area comprises three zones: the overlying

layer, the natural gas hydrate reservoir, and the underlying layer. The permeability of the overlying layer and the underlying layer is zero and no flow happens. All the layers are horizontal according to Qin et al. (2020) [32]. Based on the differing geological conditions across the vertical layers, the z-direction is discretized into four overlaying layers, five hydrate layers, five three-phase layers, three aqueous layers, and four underlying layers, with thicknesses of 40 m, 35 m, 15 m, 27 m, and 40 m, respectively. A well is employed at the center of the whole zone for pressure reduction, penetrating through the three-phase layers. The whole domain is discretized into a grid system of 56 × 56 × 21, with each grid cell measuring 10 m in length and width. The top layer is situated at a depth of 1495 m, with a temperature of 12.19 °C and a geothermal gradient of 0.051 °C·m^{-1}. The bottomhole pressure is set at 4.5 MPa. In the simulation, three phases are considered—hydrate, water, and gas. The porosity will change after the hydrate decomposition and the permeability will change. In both the horizontal and vertical directions of the simulation model, the boundary condition is closed for flow. In the simulation, the phase transition model is firstly established and the phase transition curves are drawn. Then, the k values [33] under certain pressures and temperatures are calculated. Finally, the whole simulation can be run for the first time. The real data setting in the simulation refers to the work of Qin et al. (2020) [32]. The simulation software is CMG 2021, which can achieve gas hydrate production by solving a nonlinear partial differential equation. Three-field parameters are solved, including pressure, temperature, and saturation. The simulator of CMG-STARS is chosen as the simulation tool as it can deal with phase states and analyze gas production behavior. The basic governing equations are sourced from previous research [33–35].

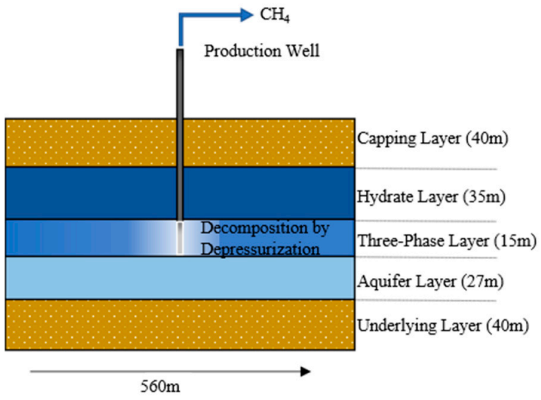


Figure 2. A schematic diagram of an NGH production test model.

Table 1 presents the required geological parameters, while Table 2 outlines the chemical reaction kinetic parameters for CH_4 hydrate decomposition.

Table 1. Geological parameters of NGH production test model [32].

Parameters	Number of Layers				
	Capping Layer	Hydrate Layer	Three-Phase Layer	Aquifer Layer	Underlying Layer
Permeability/(10^{-3} μm^2)	0	2.9	1.5	7.4	0
Porosity	0	0.35	0.33	0.32	0
Temperature/°C	12.19	14.23	16.02	16.78	18.157
Pressure/MPa	14.25	14.65	15	15.15	15.42
Water Saturation	0	0.66	0.526	0.922	0
Gas Saturation	0	0	0.164	0.078	0
Hydrate Saturation	0	0.34	0.31	0	0

Table 2. Kinetic parameters for CH_4 hydrate decomposition [32].

Parameters	$CH_4 \cdot nH_2O$
Molecular Weight/(kg·mol^{-1})	119.543×10^{-3}
Mas-Density/(kg·m^{-3})	919.7
Molar Density/(mol·m^{-3})	7693.47
Reaction Frequency Factor/(mol·day^{-1}·kPa^{-1}·m^{-2})	1.071×10^{13}
Specific Surface Area/(m^2·m^{-3})	3.750×10^5
Activation Energy/(J·mol^{-1})	81,084.2
Reaction Enthalpy/(J·mol^{-1})	51,858

2.3. History Matching

Based on the first NGH test data collected from the Shenhu area of the South China Sea in 2017, the test lasted for a total of 60 days, with a cumulative gas production of 30.9×10^4 m^3, an average daily gas production of 5151 m^3. Table 3 presents the detailed gas production data from the NGH production test.

Table 3. Gas production data from NGH production test [32].

Production Duration/Days	Cumulative Gas Production/m^3	Average Gas Production Rate/(m^3·d^{-1})
0–8	12.80	16,000
8–16	16.00	4000
16–22	18.37	3950
22–31	21.08	2978
31–42	23.50	2200
42–60	30.90	3611

Utilizing the gas production data from the test and the cumulative gas production simulated by the constructed model, production history matching and model validation are performed. The cartesian grids are refined around the wellbore. For the history matching, the permeability of the grid around the well is adjusted as the permeability changes after the drilling effect. The grid permeability is set to be 4.5 mD, which the well is located in. After the modification, the simulation results are matched with the test production results and prove the validity of the model. The mathematical model demonstrates similarity to the actual engineering results, with conclusions aligning closely and exhibiting good fitting effects that can be used for sensitivity analysis. The fitting result is illustrated in Figure 3.

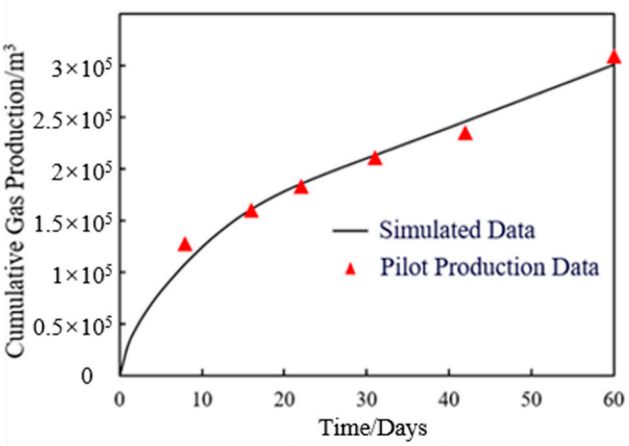


Figure 3. A history-matching curve.

3. Results and Discussion

Based on the geological model established using hydrate production parameters from the Shenhu area of the South China Sea in 2017, numerical simulation studies on single vertical well depressurization production were conducted using three representative homogeneous sediments: montmorillonite, kaolin, and silt, as well as hydrate-bearing sediments from the Shenhu area of the South China Sea (SCS). These studies were combined with phase equilibrium curves under different conditions to investigate phase change parameters' effects on gas production.

3.1. Gas Hydrate Phase Transition Models and Curves

According to the unified phase transition model considering capillary action, surface adsorption, and salinity, the temperature reduction can be calculated using the following equation [36]:

$$\frac{\Delta T_{\text{dep}}}{T_{\text{bulk}}} = \frac{n_h V_w}{\Delta H_h} \cdot a^{-1} \left[\left(\frac{w - w_r}{w_s - w_r} \right)^{\frac{1}{m}} - 1 \right]^{1-m} + \frac{n_h V_w}{\Delta H_h} \cdot RT \sum_{i=1}^{N} C_i \cdot \frac{w}{w - w_r}. \quad (1)$$

The term $\frac{n_h V_w}{\Delta H_h} \cdot a^{-1} \left[\left(\frac{w - w_r}{w_s - w_r} \right)^{\frac{1}{m}} - 1 \right]^{1-m}$ represents the hydrate phase equilibrium inhibition caused by the micro–nano capillary effect and surface adsorption, while the term $\frac{n_h V_w}{\Delta H_h} \cdot RT \sum^{i=1} C_i \cdot \frac{w}{w - w_r}$ represents the hydrate phase equilibrium inhibition caused by soluble salts. In the above equation, a is the water activity; ΔH_h is the enthalpy of hydrate dissociation, J/mol; R is the gas constant J/(mol·K); T is the system temperature, K; T_{bulk} is the phase equilibrium temperature of bulk hydrates, K; n_h is the hydration number; ΔT_{dep} is the hydrate dissociation temperature depression; V_w is the molar volume of water; w is the water content; w_r is the saturated water content in sediments; w_s is the residual water content in sediments; C_i is the molar concentration of the ion i; and N is the number of ion species in the salt solution.

The proposed model requires curve fitting to determine the unknown parameters. First, the parameters of the model are calculated using data from pure water sediments, and the parameters obtained through curve fitting, which can be found in reference [36]. a, m, m, w_s are obtained by experimental matching and verified using the experiment results.

Similarly, the accuracy of the model can also be validated by using the hydrate dissociation conditions of sediments [36]. Table 4 summarizes the phase equilibrium calculation parameters across various models and they can be examined by fitting the experiment results. This facilitates the integration with numerical simulation model results to analyze the gas production dynamics of sediments under different conditions.

Table 4. Parameters of unified model for hydrate dissociation temperature reduction [36].

Sample	a	m	w_r	w_s	R^2
Silty Sand	2.069×10^{-5}	0.4927	0.0078	0.3741	0.9975
Kaolinite	2.940×10^{-6}	0.6136	0.0373	0.3665	0.9957
Montmorillonite	5.708×10^{-7}	0.5490	0.1164	0.4472	0.9895
South China Sea Sediments	7.353×10^{-7}	0.5416	0.0627	0.4162	0.9818

Figure 4 shows the phase equilibrium curves under different pure water saturations for South China Sea sediments, montmorillonite, silty sand, and kaolinite. It can be seen that as the water content decreases, the equilibrium temperature also decreases. The water

content has a larger effect on South China Sea sediments and montmorillonite (MMT). The effect on silty sand and kaolinite is small. Figure 5 shows the phase equilibrium curves under different salinities. As can be seen, the salinities (NaCl) and water contents lead to different equilibrium pressure levels and temperatures. These curves are then put into the simulator and used to calculate the k value to judge whether the hydrate will decompose.

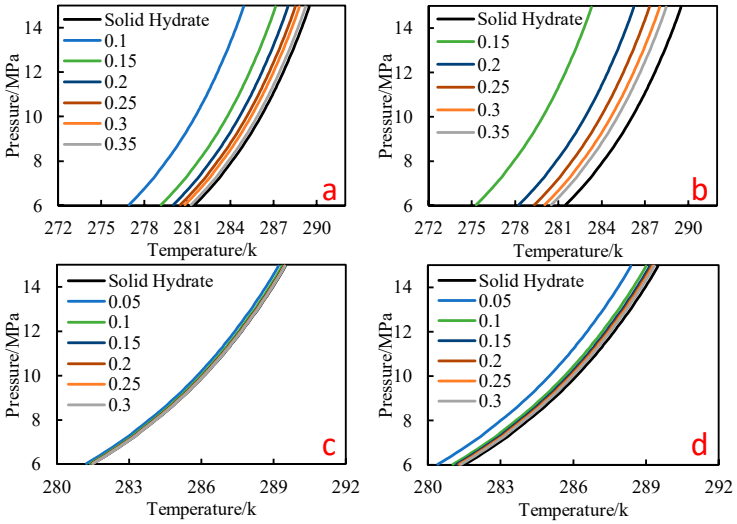


Figure 4. The temperature–pressure curves for hydrate dissociation conditions in sediments under different pure water saturations ((**a**) South China Sea sediments; (**b**) montmorillonite; (**c**) silty sand; (**d**) kaolinite).

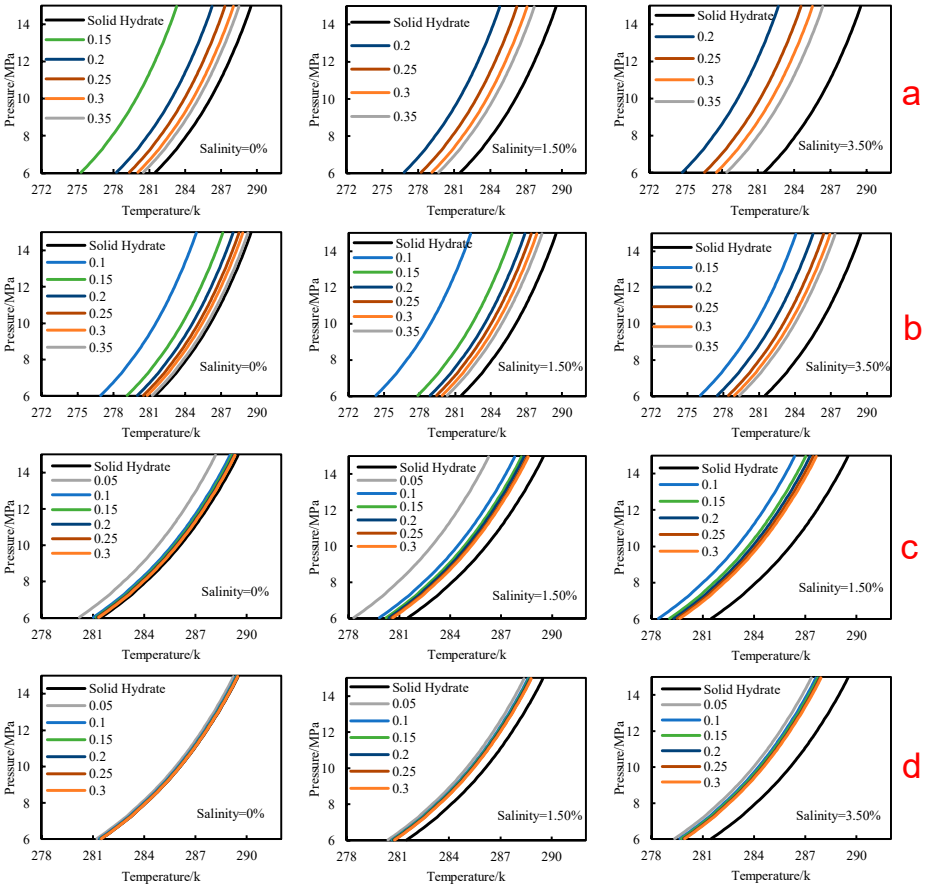


Figure 5. The temperature–pressure curves for hydrate dissociation conditions in sediments with various salinities (NaCl) and water saturations ((**a**) montmorillonite; (**b**) South China Sea sediments; (**c**) kaolinite; (**d**) silty sand).

3.2. Gas Production Performance of Different Sediments

Figure 6 shows the phase equilibrium curves that were created without considering salinity. Figure 7 shows the hydrate saturation distributions. Figure 8 shows the cumulative gas production volumes of four different sediments (MMT, South China Sea sediments, kaolinite, and silty sand) when the water content is 0.3.

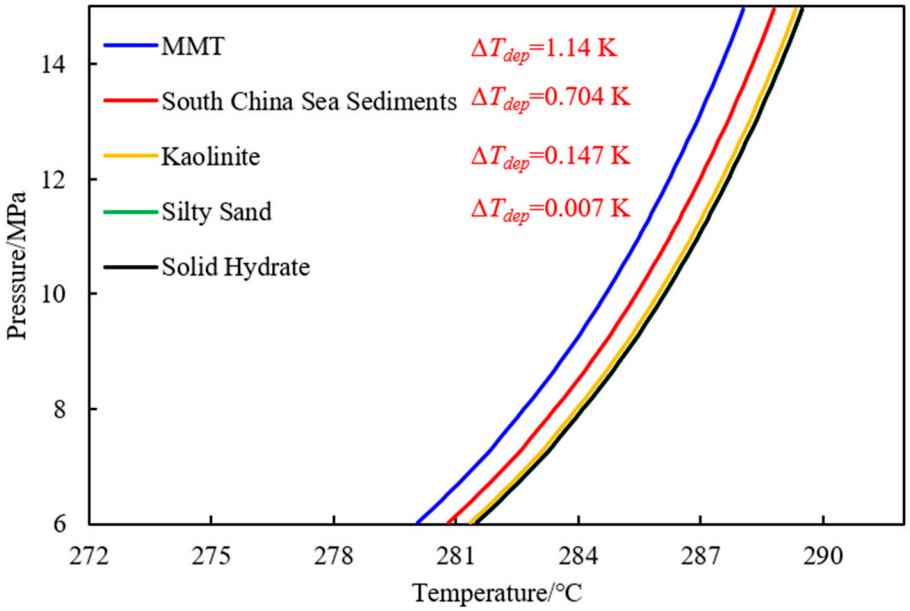


Figure 6. The phase equilibrium curves of different sediment phases with a water content of 0.3.

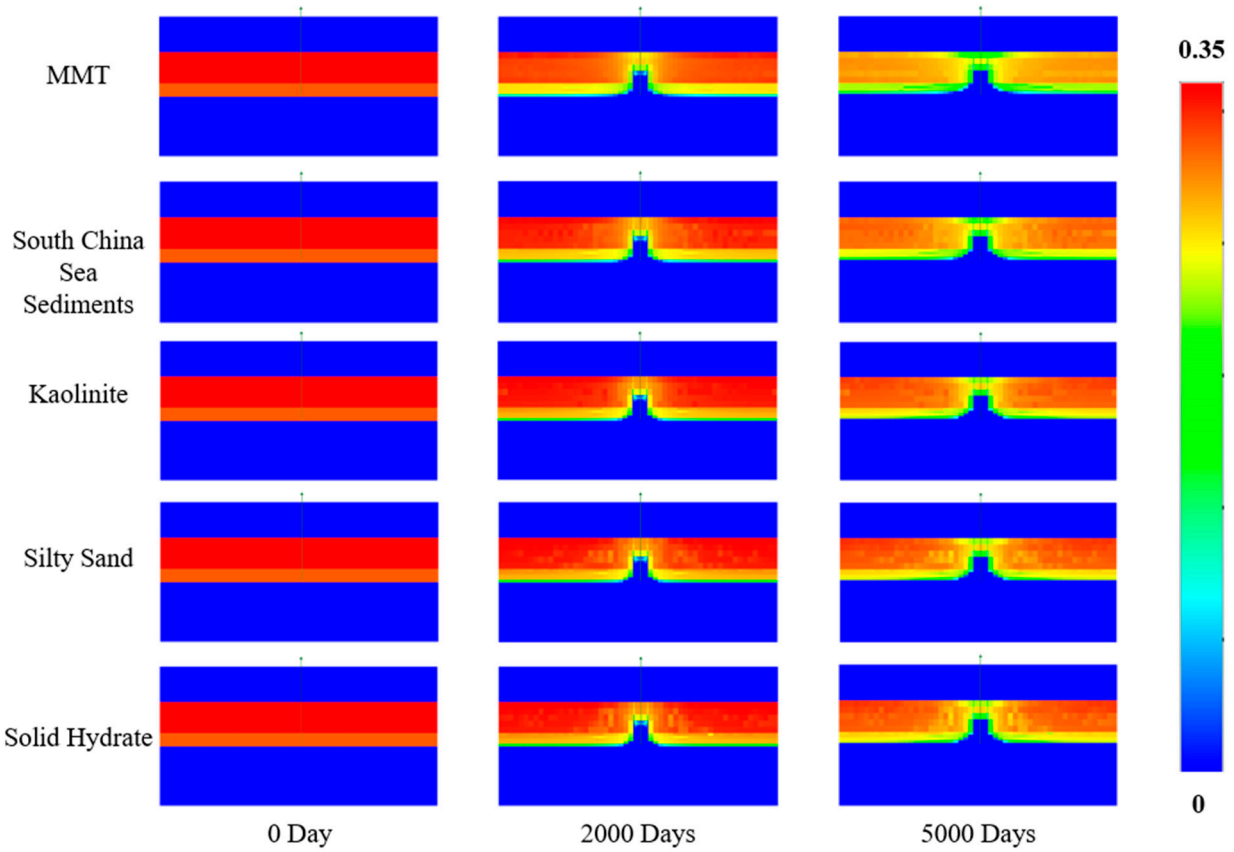


Figure 7. The hydrate saturation distributions of different sediments with a water content of 0.3.

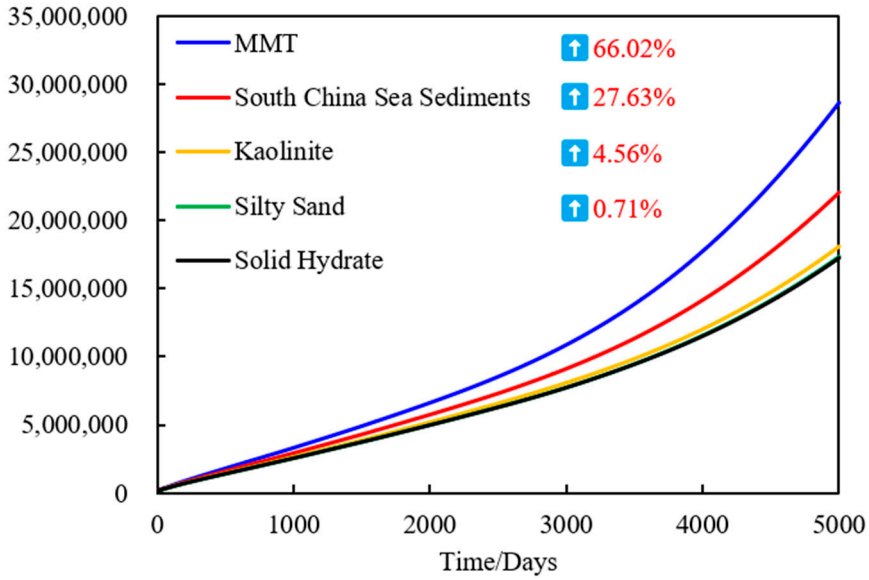


Figure 8. Gas production volumes from different sediment types with a water content of 0.3.

As shown in Figure 6, the phase equilibrium temperatures of the other sediment types are reduced compared to solid hydrates. The degrees of reduction in phase equilibrium temperature, from the most significant to the least, adhere to the following order: montmorillonite, South China Sea sediments, kaolinite, and silt. The primary reason for this is that the combined effects of capillary action and surface adsorption make montmorillonite exhibit the most significant inhibiting effect on hydrate phase equilibrium, followed by SCS sediments, then kaolinite, and finally silt, which causes the least inhibition. As shown in the hydrate saturation distributions in Figure 7, at the same time, montmorillonite has the lowest hydrate saturation, followed by SCS sediments, then kaolinite, and silt has the highest hydrate saturation. Therefore, as seen in Figure 8, montmorillonite has the largest increase in cumulative gas production, which is about 2.8×10^7 m^3 compared to solid hydrates, while silt has the smallest increase. The phase equilibrium temperature refers to the lowest temperature at which natural gas hydrates can remain stable without decomposing under a specific amount of pressure. When the ambient temperature is lower than the hydrate's phase equilibrium temperature, the hydrate tends to remain in a stable state. However, if the ambient temperature gradually rises and exceeds the phase equilibrium temperature, the hydrate's stability will be compromised, leading to decomposition. Therefore, a lower phase equilibrium temperature means that hydrates may reach their decomposition critical point at lower temperatures, making them more prone to decomposition.

3.3. Gas Production Performance at Different Water Saturations Under Pure Water Conditions

Taking South China Sea (SCS) sediments as an example, and without considering salinity, numerical simulations were conducted by varying the water content of the sediments to 0.2, 0.25, 0.3, and 0.35. This analysis focused on the phase equilibrium curves, hydrate saturation distributions, and cumulative gas production volumes of SCS sediments with different water contents.

Figure 9 indicates that as the initial water content decreases, the phase equilibrium temperature drops more significantly, the hydrate saturation at the same time point decreases, and the gas production volume increases. This is because a lower initial water content leads to a further reduction in water activity due to the additional retardation effect of capillary surface tension [37]. During the hydrate decomposition process, decreased water activity means a reduction in the effective capacity of water to participate in forming hydrates. When the initial water content in the system is higher, although capillary action

also reduces water activity, this effect is relatively minor due to the larger total amount of water. However, when the initial water content is lower, the reduction in water activity has a more pronounced inhibitory effect on hydrate formation. Additionally, when the initial water content is low, the number of water molecules that can be adsorbed is significantly reduced after adsorption sites are occupied by impurities, severely inhibiting hydrate formation and causing a decrease in the phase equilibrium temperature. Figures 10 and 11 show the hydrate saturation distributions and gas production volumes at different water contents. High water saturation leads to lower gas production.

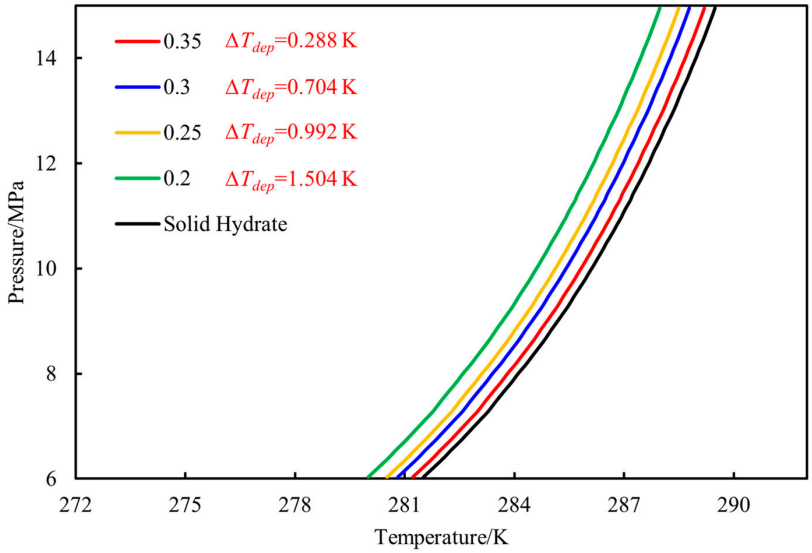


Figure 9. The phase equilibrium curves of SCS sediments with different water contents.

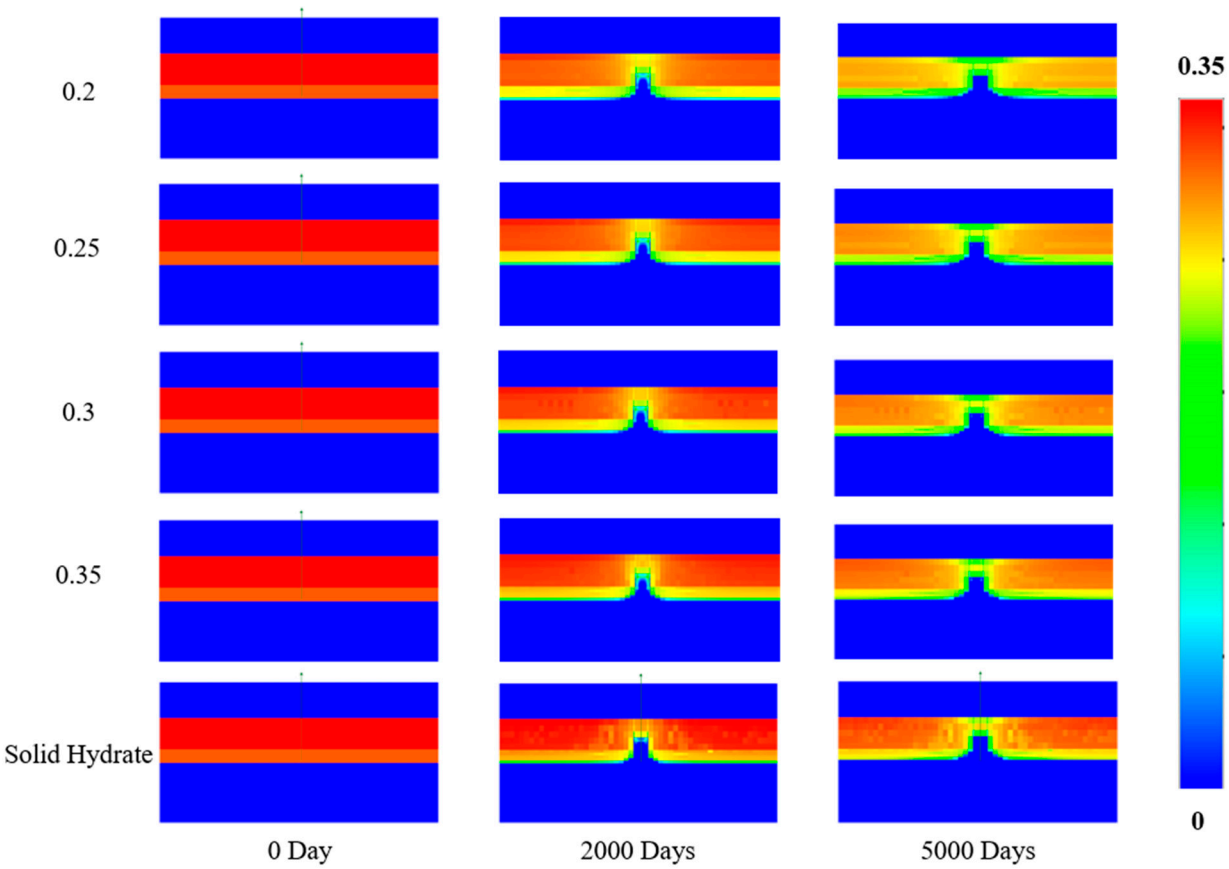


Figure 10. The hydrate saturation distributions of SCS sediments with different water contents.

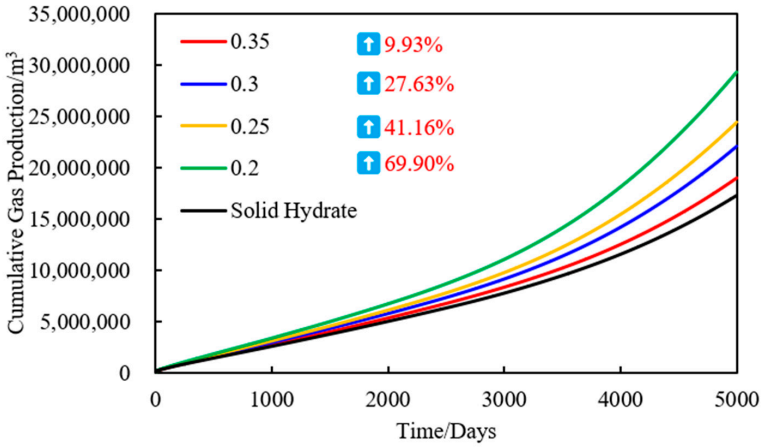


Figure 11. The gas production volumes of SCS sediments with different water contents.

3.4. Gas Production Performance of Different Sediments Considering Salinity

Considering the phase equilibrium curves of different sediments in the presence of salinity, the phase equilibrium curves, hydrate saturation distributions, and cumulative gas production volumes of four different sediments—montmorillonite, SCS sediments, kaolinite, and silt—were analyzed at a water content of 0.3 and a salinity of 1.5%.

Figure 12 shows that, compared to solid hydrates, the phase equilibrium temperatures of the other sediments are lower, with the magnitudes of decrease adhering to the following order: montmorillonite, SCS sediments, kaolinite, and silt. Figure 13 indicates that, at the same time, the hydrate saturation levels, when ordered from lowest to highest, are as follows: montmorillonite, South China Sea sediments, kaolinite, and silt. Figure 14 shows that montmorillonite experiences the largest increase in cumulative gas production compared to solid hydrates, while silt experiences the smallest increase. This is consistent with the gas production dynamics observed in different sediments without considering salinity. However, the difference is that when salinity is considered, the reduction in phase equilibrium temperature is enhanced, leading to higher gas production volumes. This is primarily due to the ionic effect caused by ions ionized from salt substances in aqueous solutions. This effect disrupts the original ionization equilibrium state, resulting in changes to the equilibrium constants of hydrated ions, which, in turn, lowers the temperature required for the formation of natural gas hydrates, weakening their stability and making them more susceptible to decomposition [37,38].

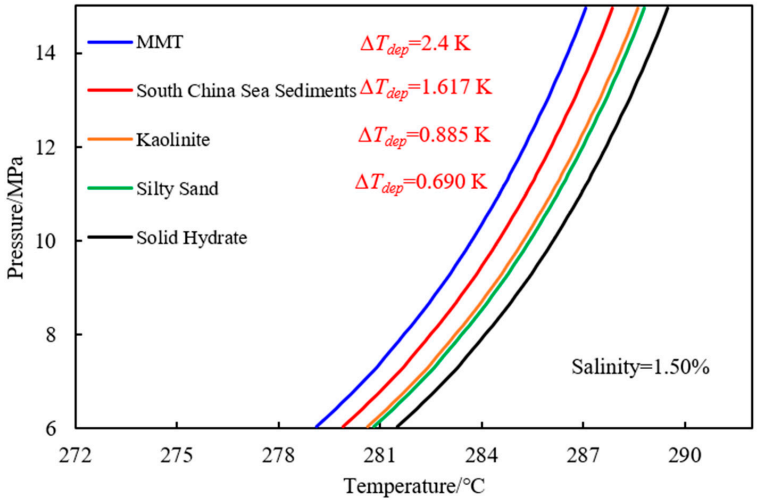


Figure 12. The phase equilibrium curves of different sediments with 0.3 water content and 1.50% salinity.

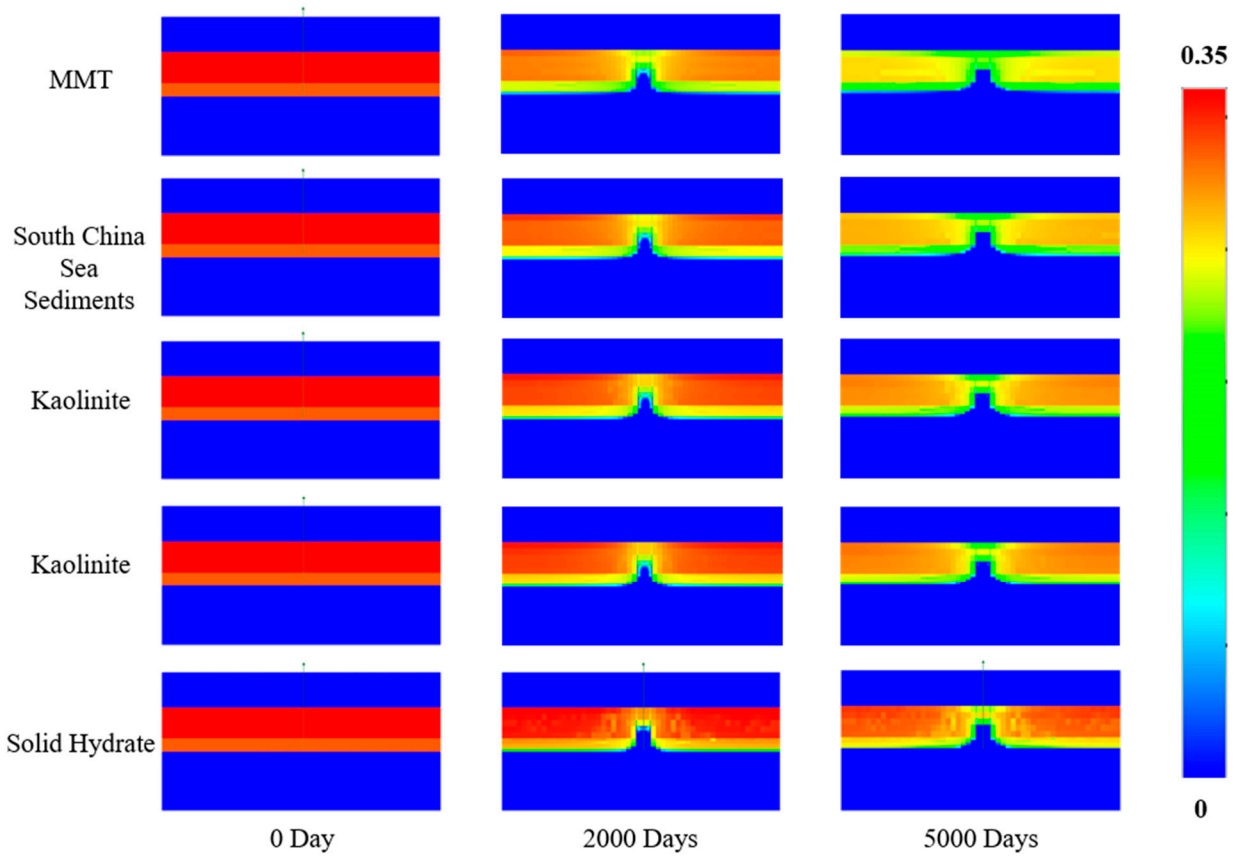


Figure 13. The hydrate saturation distributions of different sediments with 0.3 water content and 1.5% salinity.

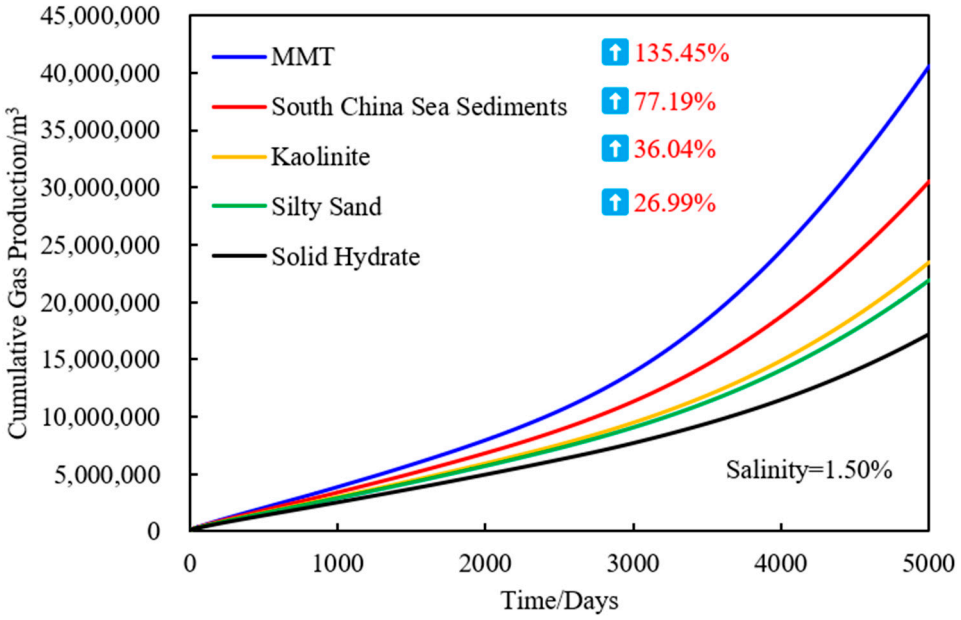


Figure 14. The gas production rates of different sediments with 0.3 water content and 1.50% salinity.

3.5. Gas Production Performance of SCS Sediments at Different Salinity Levels

Using the phase equilibrium curves of SCS sediments at different salinities, the phase equilibrium curves, hydrate saturation distributions, and cumulative gas production volumes were analyzed for salinities of 0%, 1.5%, and 3.5%.

As shown in Figures 15–17, the higher the salinity, the greater the reduction in the phase equilibrium temperature of the SCS sediments. At the same time point, higher salinity results in lower hydrate saturation, indicating faster hydrate dissociation and a higher gas production volume. This is because higher salinity has a stronger inhibitory effect on hydrate formation [39], making it easier to reach dissociation conditions and thus increasing gas production.

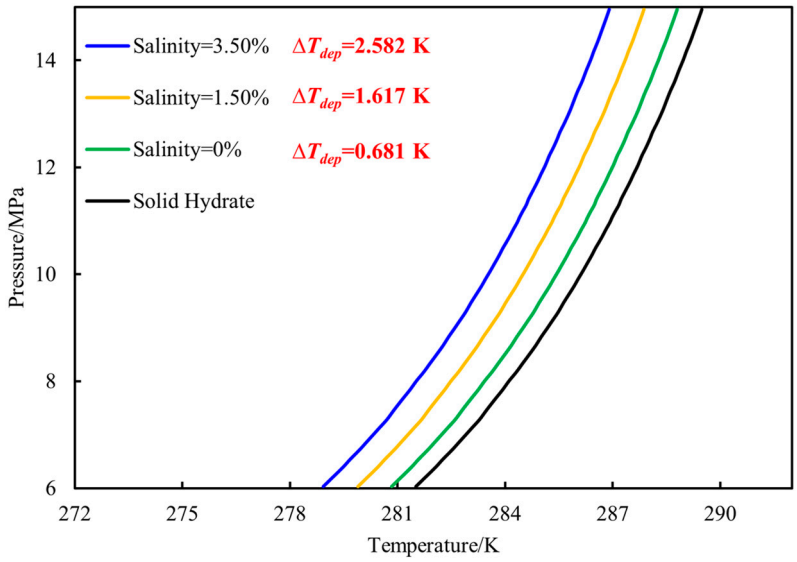


Figure 15. The phase equilibrium curves of SCS sediments with a water content of 0.3 and different salinities.

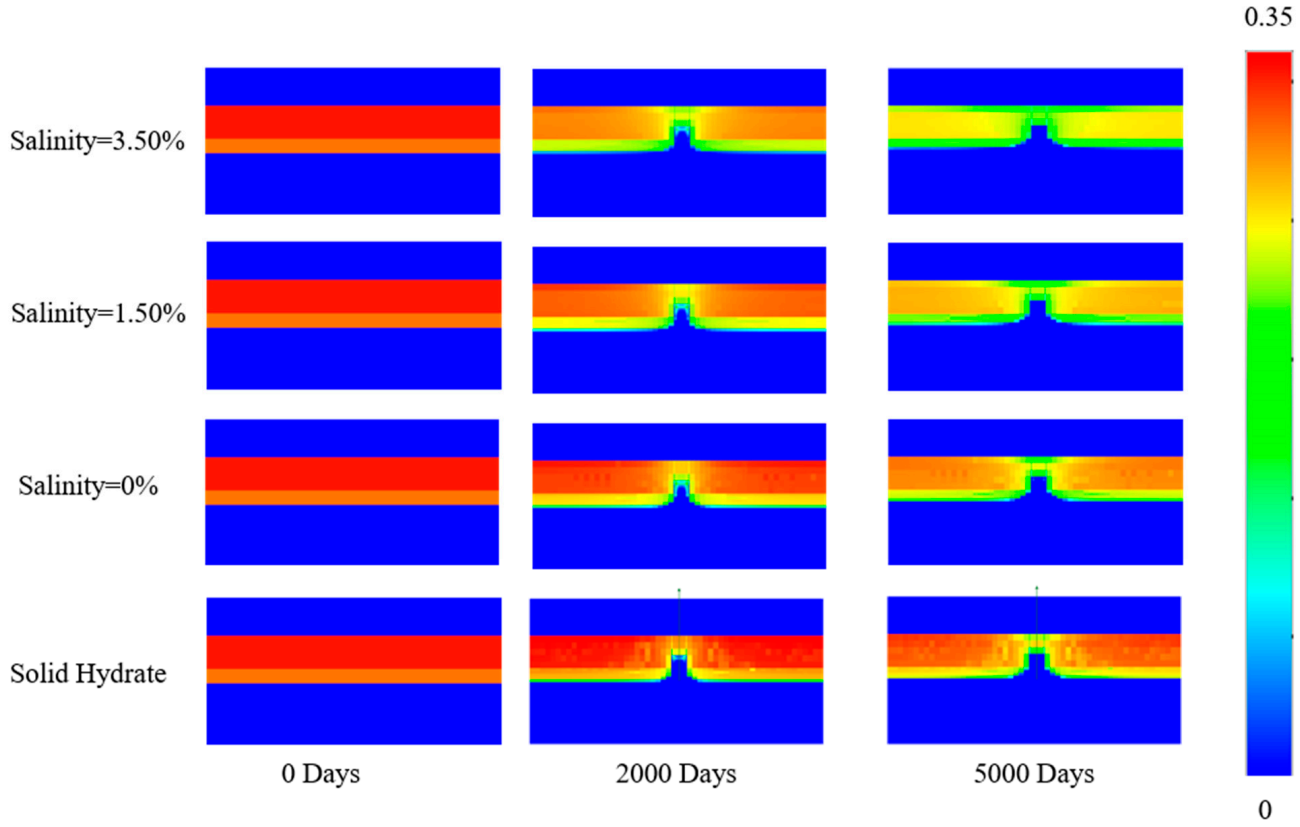


Figure 16. The hydrate saturation distributions of different salinity.

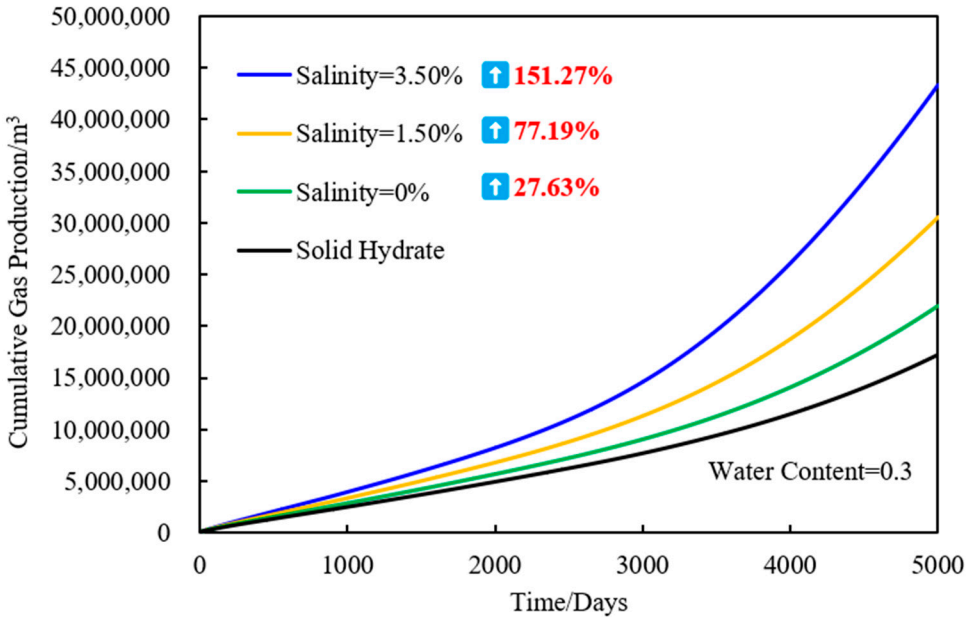


Figure 17. The gas production curves of SCS sediments with a water content of 0.3 and different salinities.

4. Conclusions

This paper establishes a numerical model for depressurization production of natural gas hydrates by using geological data from the hydrate production test conducted in the Shenhu area of the South China Sea to study the phase transition characteristics of hydrates at the field scale. The phase equilibrium is modified by considering different effect parameters. Combining the phase transition model charts of different sediments under various conditions indicates that when capillary action and surface adsorption are considered, the degrees of reduction in phase equilibrium temperature for the four studied sediments are as follows: montmorillonite > SCS sediments > kaolinite > silt soil. The lower the initial water content and the higher the salinity, the lower the phase equilibrium temperature of natural gas hydrates, resulting in increased natural gas production.

Author Contributions: Conceptualization, formal analysis, writing—original draft, project administration, funding acquisition, Q.F.; methodology, formal analysis, investigation, M.C.; data curation, supervision, validation, W.P.; writing—review and editing, L.D. All authors have read and agreed to the published version of the manuscript.

Funding: This research was funded by Research on Cross-Scale Phase Transition Characteristics and Numerical Simulation Methods for Depressurization Development of Natural Gas Hydrates (KJQZ-2023-2003) and the National Natural Science Funding (52474076).

Institutional Review Board Statement: Not applicable.

Informed Consent Statement: Not applicable.

Data Availability Statement: The data presented in this study are available upon request from the corresponding author.

Conflicts of Interest: Authors Qiang Fu, Mingqiang Chen and Weixing Pang were employed by the company China National Offshore Oil Corporation. The remaining authors declare that the research was conducted in the absence of any commercial or financial relationships that could be construed as a potential conflict of interest.

References

1. Licence, P. Clathrate Hydrates of Natural Gases, third ed. E. Dendy Sloan, A. Koh Carolyn. Chemical Industries Series. CRC Press (2007). 752 p. 130, Hardcover. *Fuel* **2008**, *87*, 3158. [CrossRef]
2. Tang, X.Y.; Chen, J.W.; Guo, Y.L.; Liang, F.C.; Wang, C. Development Status of Combustible Ice Mining and Test Production Technologies. *Nat. Gas Oil* **2020**, *38*, 7–15. [CrossRef]
3. Zhang, X.H.; Lu, X.B.; Li, P. A comprehensive review in natural gas hydrate recovery methods. *Sci. Sin. Pysica Mech. Astron.* **2019**, *49*, 34–55. [CrossRef]
4. Li, L.S.; Miao, Q. Overview of the Development of Exploration and Production Technologies for Natural Gas Hydrates. *Nat. Gas Oil* **2014**, *32*, 67–71. [CrossRef]
5. Du, W.G.; Qian, X.R.; Xie, M.C. Analysis of completion and production test technology for natural gas hydrate in Japan. *Well Test.* **2019**, *28*, 49–53. [CrossRef]
6. Zuo, R.Q.; Li, Y. The Research and Successful Production Test for NGH in Alaska North Slope, USA. *Explor. Eng. Rock Soil Drill. Tunneling* **2017**, *44*, 1–17. [CrossRef]
7. Shi, D.; Zheng, J.W. The status and prospects of research and exploitation of natural gas hydrate in the world. *Adv. Earth Sci.* **1999**, *14*, 330–339. [CrossRef]
8. Chen, D.F.; Wang, M.C.; Xia, B. Formation condition and distribution prediction of gas hydrate in Qinghai-Tibet Plateau permafrost. *Chin. J. Geophys.* **2005**, *48*, 165–172. [CrossRef]
9. Wu, N.Y.; Zhang, H.Q.; Yang, S.X.; Liang, J.Q.; Wang, H.B. Preliminary Discussion on Natural Gas Hydrate (NGH) Reservoir System of Shenhu Area, North Slope of South China Sea. *Nat. Gas Ind.* **2007**, *27*, 1–6. [CrossRef]
10. The trial production of natural gas hydrates in the South China Sea has successfully concluded. *Equip. Geotech. Eng.* **2017**, *18*, 3. [CrossRef]
11. Jiang, H.; Cao, X.X. Exploration and Development of Natural Gas Hydrate. *Guangzhou Chem. Ind.* **2020**, *48*, 1–2+5. [CrossRef]
12. Pang, X.Q.; Hu, T.; Pu, T.Y.; Xu, Z.; Wang, E.; Wang, W.; Li, C.; Zhang, X.; Liu, X.; Wu, Z.; et al. Risks and challenges of the industrial development of methane hydrate resources in the South China Sea. *Acta Pet. Sin.* **2024**, *45*, 1044–1060. [CrossRef]
13. Ruppel, C. Permafrost-associated gas hydrate: Is it really approximately 1% of the global system? *J. Chem. Eng. Data* **2015**, *60*, 429–436. [CrossRef]
14. Ruppel, C.D.; Kessler, J.D. The interaction of climate change and methane hydrates. *Rev. Geophys.* **2017**, *55*, 126–168. [CrossRef]
15. Qin, X.W.; Lu, C.; Wang, P.K.; Liang, Q.-Y. Hydrate phase transition and seepage mechanism during natural gas hydrate production tests in the South China Sea:A review and prospect. *Geol. China* **2022**, *49*, 749–769. [CrossRef]
16. Zang, X.Y.; Liang, D.Q.; Wu, N.Y. Research Progress on Methane Hydrate Formation Kinetics in Porous Media. *Adv. New Renew. Energy* **2015**, *3*, 131–138. [CrossRef]
17. Liu, Y.Y. Molecular Simulation Study on the Micro-Mechanism of Natural Gas Hydrate Exploitation. Master's Thesis, China University of Petroleum (East China), Qingdao, China, 2019. [CrossRef]
18. Almenningen, S.; Flatlandsmo, J.; Fernø, M.A.; Geir, E. Production of Sedimentary Methane Hydrates by Depressurization. In Proceedings of the Spe Bergen One Day Seminar, Bergen, Norway, 20 April 2016. [CrossRef]
19. Wang, L.H.; Zang, X.Y.; Guan, J.A.; Liang, D.Q. Microscopic decomposition characteristics of methane hydrate in nanopores. *Petrochem. Technol.* **2020**, *49*, 153–159.
20. Kuang, Y.M. Research on the Impact of Microscopic Phase Transition of Hydrates within Porous Media on Gas-Water Migration. Ph.D. Thesis, Dalian University of Technology, Dalian, China, 2021. [CrossRef]
21. Guan, W.; Yang, H.L.; Lu, H.L. Research on Factors Influencing the Phase Equilibrium of Natural Gas Hydrates in Porous Media. *Earth Sci. Front.* **2024**, 1–19. Available online: http://kns.cnki.net/kcms/detail/11.3370.P.20240624.1437.002.html (accessed on 19 October 2024).
22. Wang, S.H.; Song, H.B.; Yan, W. The change of external conditions effects on the phase equilibrium curve of gas hydrate and the thickness of hydrate stability zone. *Prog. Geophys.* **2005**, *20*, 761–768. [CrossRef]
23. Su, X.; Li, Y.; Gao, L.; Zhang, L. The Effect of Gas Component on Formation Temperature of Hydrate. *Nat. Gas Explor. Dev.* **2008**, *31*, 64–66. [CrossRef]
24. Li, P.F.; Lei, X.H.; Hao, X.; Xiang, H. A review on researches on factors affecting gas hydrate phase equilibrium. *Nat. Gas Chem. Ind.* **2012**, *37*, 12–17. [CrossRef]
25. Ruan, X.K.; Li, X.S.; Yang, J.M.; Yu, F. Influences of gas hydrate reformation and permeability changes on depressurization recovery. *Acta Pet. Sin.* **2015**, *36*, 612–619. [CrossRef]
26. Han, D.Y. Multiscale Study on the Seepage Characteristics During Hydrate Phase Transition Processes in Porous Media. Ph.D. Thesis, Dalian University of Technology, Dalian, China, 2020. [CrossRef]
27. Zhou, J.; Gu, J.T.; Xu, H.P.; Wang, Z.T.; Wang, Q.H.; Ma, Y.G. Analysis and numerical simulation of factors affecting natural gas hydrate phase equilibrium. *Pet. Eng. Constr.* **2021**, *47*, 48–54. [CrossRef]

28. Xu, T.; Zhang, Z.B.; Li, S.D.; Li, X.; Lu, C. Three-Dimensional Numerical Simulation Study on the Impact of Permeability Performance of Natural Gas Hydrate Geological Systems on Hydrate Decomposition Behavior. In Proceedings of the 2021 China Earth Sciences Joint Academic Conference (Volume 38)—Special Topic 113: Young Scholars Forum on Natural Gas Hydrate Development, Online, 6 December 2021; Institute of Geology and Geophysics, Chinese Academy of Sciences; Oil and Gas Resources Center, China Geological Survey: Beijing, China, 2021; Volume 4. [CrossRef]
29. Chen, X. Numerical Simulation Study of Depressurization-Induced Decomposition of Natural Gas Hydrates in Microchannels. Master's Thesis, Harbin Engineering University, Harbin, China, 2021. [CrossRef]
30. Farahani, M.V.; Hassanpouryouzband, A.; Yang, J.; Tohidi, B. Insights into the climate-driven evolution of gas hydrate-bearing permafrost sediments: Implications for prediction of environmental impacts and security of energy in cold regions. *Rsc Adv.* **2021**, *11*, 14334–14346. [CrossRef] [PubMed]
31. Farahani, M.V.; Hassanpouryouzband, A.; Yang, J.; Tohidi, B. Development of a coupled geophysical–geothermal scheme for quantification of hydrates in gas hydrate-bearing permafrost sediments. *Phys. Chem. Chem. Phys.* **2021**, *23*, 24249–24264. [CrossRef]
32. Qin, X.; Liang, Q.; Ye, J.; Yang, L.; Qiu, H.; Xie, W.; Liang, J.; Lu, C.; Lu, H.; Ma, B.; et al. The response of temperature and pressure of hydrate reservoirs in the first gas hydrate production test in South China Sea. *Appl. Energy* **2020**, *278*, 115649. [CrossRef]
33. Pooladi-Darvish, M.; Hong, H. Use of formation pressure test results over a hydrate interval for long-term production forecasting at the Mount Elbert Gas Hydrate Stratigraphic Test Well, Alaska North Slope: Implications of uncertainties. *Mar. Pet. Geol.* **2011**, *28*, 535–545. [CrossRef]
34. Li, S.; Li, S.; Zheng, R.; Li, Q.; Pang, W. Strategies for gas production from Class 2 hydrate accumulations by depressurization. *Fuel* **2021**, *286*, 119380. [CrossRef]
35. Giraldo, C.; Klump, J.; Clarke, M.; Schicks, J.M. Sensitivity analysis of parameters governing the recovery of methane from natural gas hydrate reservoirs. *Energies* **2014**, *7*, 2148–2176. [CrossRef]
36. Liu, Z.; Wang, Z.; Chen, L.; Li, X.; Sun, B. Experimental and modeling investigations of hydrate phase equilibria in natural clayey-silty sediments. *Chem. Eng. J.* **2022**, *449*, 137557. [CrossRef]
37. Yang, M.J.; Song, Y.C.; Liu, Y. Effects of porous media and salinity on phase equilibrium of methane hydrates. *J. Dalian Univ. Technol.* **2011**, *51*, 5. [CrossRef]
38. Chen, Y.; Yan, T.; Sun, X.F.; Qv, J.; Yao, D. Study on influence factors and rules of gas hydrate phase equilibrium based on multiflash software. *J. Chengdu Univ. Technol. (Sci. Technol. Ed.)* **2020**, *47*, 358–366. [CrossRef]
39. Gu, F.; Zhao, H.J.; Wang, S.L. Study on Phase Equilibrium Conditions of Natural Gas Hydrate in System Containing Salt. *Chem. Eng. Oil Gas* **2008**, *37*, 149–151. [CrossRef]

Disclaimer/Publisher's Note: The statements, opinions and data contained in all publications are solely those of the individual author(s) and contributor(s) and not of MDPI and/or the editor(s). MDPI and/or the editor(s) disclaim responsibility for any injury to people or property resulting from any ideas, methods, instructions or products referred to in the content.